Catalysis Letters
https://doi.org/10.1007/s10562-018-2416-2

# Aldol Condensation of Benzaldehyde and Heptanal Over Zinc Modified Mixed Mg/Al Oxides

**Zdeněk Tišler[1] · Eva Vrbková[1,2] · Jaroslav Kocík[1] · David Kadlec[1] · Eliška Vyskočilová[2] · Libor Červený[2]**

Received: 15 February 2018 / Accepted: 14 May 2018


**Abstract**
Several types of zinc modified Mg–Al layered double hydroxides were prepared. Zinc was incorporated into catalyst structure using different methods—coprecipitation, kneading or impregnation. Characterization of all solid catalysts was performed using different techniques. Acido–basic properties of prepared materials were investigated using ammonia (or carbon dioxide) temperature programmed desorption. The activity of the prepared samples was compared with pure Mg–Al oxide with Mg:Al ratio 3:1 in aldol condensation of benzaldehyde and heptanal. The influence of temperature (80–120 °C) on the reaction course was monitored. Heptanal conversion and selectivity to two main products, i.e. 2-pentylcinnamylaldehyde (jasmine aldehyde) and 2 pentylnon-2-enal, were evaluated. Zinc modified catalysts exhibited under the same conditions 15–20% higher yields of the desired jasmine aldehyde.

**Graphical Abstract**

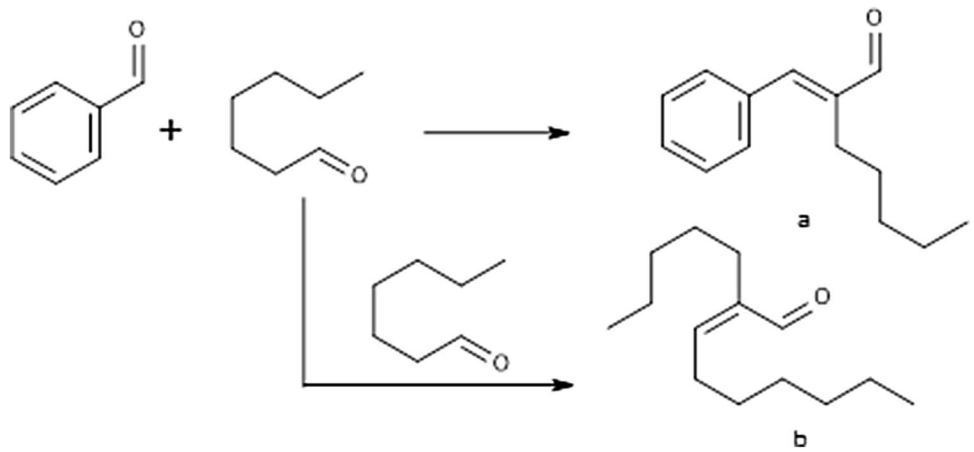


**Keywords** Layered double hydroxide · Zn–Mg–Al mixed oxides · Jasmine aldehyde · Aldol condensation

## 1 Introduction

Aldol condensation between substituted 4-alkylaldehyde and linear aldehydes is a way to produce different fragrances. This type of substances is frequently used in the perfume industry due to its stability in basic environment, which makes the compounds perfect for use in a number of detergents, shampoos and soaps. In industry, these aldol condensations are usually catalyzed by inorganic hydroxides.

✉ Eva Vrbková
eva.vrbkova@vscht.cz

[1] Unipetrol Centre of Research and Education, Inc., Areál Chempark 2838, Záluží 1, 436 70 Litvínov, Czech Republic

[2] University of Chemistry and Technology Prague, Technická 5, Dejvice, 166 28 Prague 6, Czech Republic

Published online: 23 May 2018

However, this brings along certain drawbacks, such as the use of corrosive mixtures and the production of large amounts of waste salts. The use of heterogeneous basic catalysts is promising because it offers a simple catalyst separation or even the potential to reuse the catalyst. In aldol condensation of benzaldehyde with heptanal, a wide number of different heterogeneous catalysts have already been used; among them, amino functionalized silicas [1], acid functionalized silicas [2, 3], magnesium organosilicates [4], chitosan grafted hydrotalcites [5], potassium or caesium modified solid supports [6], metal organic frameworks [7] or mixed Mg–Al oxides [8–16] seem to be very promising catalysts. In this work, Mg–Al–Zn oxides prepared by different methods were chosen to perform aldol condensation of benzaldehyde with heptanal. Addition of zinc to the catalyst structure can enhance its Lewis acidity and increase its activity in aldol condensation, which is typically both acid and basic catalysed [17].

Hydrotalcites (HTCs, also layered double hydroxides LDHs) are a widely used group of materials with the structure derived from natural mineral brucite. The chemical composition of hydrotacites can be represented by the general formula $[M^{II}_{1-x}M^{III}_{x}(OH)_2]^{x+}\cdot[A^{n-}_{x/n}\cdot y\ H_2O]^{x-}$, where $M^{II}$ and $M^{III}$ represent divalent and trivalent metal cation respectively, and $A^{n-}$ stands for n-valent anion. Laminarity of these materials is caused by alternating the positive hydroxide layers containing metal $Me^{II+}$ and $Me^{III+}$ ions with the negative layers of hydrated anions in interlayer space. Individual layers are connected via weak hydrogen bonds. Calcination of hydrotalcites creates mixed oxides, which have no more laminar structure. During calcination, water molecules and carbonate anions are eliminated from structure and basic Lewis sites are formed. The laminar structure of mixed oxide can be re-established by rehydration, which generates again Brönsted basic sites (this behaviour is denoted as memory effect) [18–21].

In this work aldol condensation of benzaldehyde and heptanal yielding jasmine aldehyde and 2-pentylnon-2-enal was studied as a model reaction to explore the catalytic properties of a number of Zn–Mg–Al catalysts.

## 2 Materials and Method

### 2.1 Synthesis of Mixed Oxides

Zn–Mg–Al LDH´s with Zn:Mg:Al molar ratio from 0:3:1 to 3:0:1 were synthesized by co-precipitation method at constant pH value (pH 9.5) and constant temperature (T = 60 °C). The zinc hydroxide was synthesized by precipitation under the same conditions. The preparation procedure involved mixing of aqueous solutions of nitrates consisting of zinc nitrate $Zn(NO_3)_2\cdot6H_2O$, magnesium nitrate $Mg(NO_3)_2\cdot6H_2O$ and aluminum nitrate $Al(NO_3)_3\cdot9H_2O$ (all Lachner, p.a. purity) ($c_{Zn+Mg+Al}$ = 1 mol/dm$^3$), and a basic solution containing potassium carbonate $K_2CO_3$ (Penta, p.a. purity) and potassium hydroxide KOH (Lachner, p.a. purity) ($c_{KOH}$ = 2 mol/dm$^3$ + $c_{K2CO3}$ = 0.2 mol/dm$^3$). After precipitation the solids were isolated by press-filtration using paper filter plate S15N (Hobra); the filter cake was washed by demineralised water to neutral pH and dried in oven overnight at 65 °C. Samples were denoted as ZA, MA, Z and series with different Zn content ZMA-1 to ZMA-6.

Four modified samples were prepared by post-synthesis modification of prepared Mg–Al LDH (MA sample). The wet part of filter cake from MA sample synthesis was used for preparation of sample with ZnO. The wet filter cake was 15 min kneaded with powdered ZnO (Lachner, p.a. purity), and prepared sample was thereafter dried overnight at 65 °C. The sample was denoted as ZMA-7.

ZMA-8 and ZMA-9 samples were prepared by incipient wetness impregnation method. The sample ZMA-8 was prepared by impregnation of calcined MA (calcination in open air 3 h at 450 °C) by solution of zinc nitrate $Zn(NO_3)_2\cdot6H_2O$. The impregnated sample was dried overnight at 65 °C. The same process, but with dried MA, was used for preparation of the next sample. MA was only dried overnight at 120 °C, and impregnated by solution of zinc nitrate $Zn(NO_3)_2\cdot6H_2O$. After impregnation it was dried overnight at 65 °C and denoted as ZMA-9.

The last sample was prepared by homogenous precipitation of zinc hydroxide on Mg–Al LDH surface. The MA, dried overnight at 120 °C, was suspended at 70 °C in 300 ml of demineralised water and 200 ml of zinc nitrate, and urea solution was dropwise added (molar ratio of zinc nitrate to urea was 1:5). The suspension of LDH was heated for 4 h to reflux temperature. After this time the suspension was cooled, filtered, washed by demineralised water and left to dry overnight at 65 °C. The sample was denoted as ZMA-10. The zinc content of all modified samples was calculated to the target Zn:Mg:Al ratio 0.5:2.5:1.0.

The calcined versions of all samples were denoted with "C" before the name of the sample.

Equation of co-recipitation:

$$6Me(NO_3)_2 + 2Al(NO_3)_3 + 16KOH + K_2CO_3 + 4H_2O = Me_6Al_2(OH)_{16}CO_3\cdot 4H_2O + 18KNO_3$$

Me = Mg and Zn

Equation of precipitation:

$$Zn(NO_3)_2 + 2KOH = Zn(OH)_2 + 2KNO_3$$

Equations of homogenous precipitation:

$$(NH_2)_2CO + H_2O = 2NH_3 + CO_2$$

$$CO_2 + H_2O = H_2CO_3$$

$$H_2CO_3 = 2H^+ + CO_3^{2-}$$

$$5Zn^{2+} + 2CO_3^{2-} + 6OH^- = Zn_5(CO_3)_2(OH)_6$$

### 2.2 Characterization

The crystallographic structure of the precursors and catalysts was determined by examining the X-ray diffraction (XRD) patterns of the powder samples obtained by using D8 Advance ECO (Bruker) applying $CuK_{\alpha}$ radiation ($\lambda = 1.5406$ Å). The step size of 0.02° and the step time of 0.5 s were used. The patterns were collected over a 2θ range of 5°–70° and evaluated by using the Diffrac.Eva software with the Powder Diffraction File database (PDF 2–2002, International Centre for Diffraction Data).

The specific surface areas (BET) of the catalysts were determined by $N_2$ adsorption/desorption at − 196 °C by using Autosorb iQ (Quantachrome Instruments). All samples were dried before the analysis in a glass-cell at 110 °C (200 °C for calcined materials) under vacuum for 16 h.

SEM images were obtained by using a scanning electron microscope (SEM) JSM-7500F (JEOL Ltd.) with a cold cathode—field emission SEM (parameters of measurements: 1 kV, GB high mode).

Acid–base properties of materials were characterized by means of $CO_2$ and $NH_3$ temperature programmed desorption (TPD) using Autochem 2950 HP (Micromeritics Instrument Corporation). Typically, a 100 mg sample in a quartz U-tube reactor was pretreated in He to 450 °C with temperature ramp of 10°C/min. In the case of $NH_3$-TPD, the sample was cooled to 50 °C and then saturated by ammonia (flow 25 ml/min, 10 vol% $NH_3$/He for 30 min). Subsequently, the gas was changed to helium (25 ml/min) in order to remove physically/weakly adsorbed ammonia [flushing out until the baseline was constant (60 min)]. After this procedure the temperature was increased to 450 °C at a rate of 15°C/min to obtain $NH_3$-TPD curves. In the case of $CO_2$-TPD, the pretreatment was the same as for $NH_3$-TPD. After the pretreatment the sample was cooled to 50 °C and the gas was switched to gas mixture of 10 vol% $CO_2$/He (25 ml/min). The sample was saturated by $CO_2$ for 30 min. Then the gas was changed to helium and left for 1 h at 50 °C in order to remove weakly adsorbed molecules. TPD curves were obtained by increasing the temperature from 50 to 450 °C with the ramp of 15 °C/min. The changes of gas concentration were monitored by a TCD detector.

Diffuse Reflectance Infrared Fourier Transform Spectroscopy (DRIFT) of dried and calcined samples was obtained using Nicolet iS 10 (Thermo Scientific). The sample (15 mg) was mixed with KBr (300 mg) and measured with the following parameters: number of scans 128 and resolution 2 $cm^{-1}$.

Thermogravimetric analyses (TGA) of dried LDH catalysts were obtained using TA Instruments TGA Discovery series operating at heating ramp 10°C/min from the temperature of 40–900 °C in flowing of nitrogen (20 ml/min, Linde 5.0). Approximately 15 mg of sample was heated in an open alumina crucible. Quadrupole mass detector Omni-Star GSD320 (Pfeiffer Vacuum Austria GmbH) was used for detection of fragments. Measurements were carried out by SCAN mode with voltage 1450 V of electron multiplier.

The chemical composition was verified by using an ICP-EOS Agilent 725 (Agilent Technologies Inc.). Before analysis, a 200 mg sample was dissolved in 10 $cm^3$ of $H_2SO_4$ (1:1) and heated. After dissolution, the sample was cooled down, diluted with demineralized water and heated to 100 °C for a few minutes. Finally, the solution of sample was transported to volumetric flask and measured.

### 2.3 Aldol Condensation

For the studied aldol condensation, benzaldehyde and heptanal (both Sigma-Aldrich, 97%) were used. Heptanal was freshly distilled before the reaction. The solvent used for the reaction was *N,N'*-dimethylformamide (DMF, Penta, p.a.). The catalysts were activated before the reaction by calcination (air, 450 °C, 15 h).

In a typical experiment, a 25 ml round-bottomed flask was equipped with condenser and filled up with solvent (when used, 1 ml), catalyst and benzaldehyde, and the reaction mixture was stirred vigorously and heated to the desired temperature (80–100 °C). Then heptanal was added in three portions—in minutes 0, 30 and 60 of the reaction (to suppress autocondensation of heptanal). The reactant ratio was as follows: 20 wt% of catalyst compared to heptanal amount, heptanal:benzadehyde molar ratio 1:2. A typical experiment involved: benzaldehyde (0.87 ml, 8.50 mmol), heptanal (0.60 ml, 4.25 mmol), 0.097 g of catalyst and DMF as solvent (1 ml).

Prior to analysis, the samples (4 × 0.1 ml) were centrifuged, diluted with ethanol, and then analyzed using Shimadzu GC 17A chromatograph fitted with nonpolar column ZB-5 (60 m, 0.32 mm diameter, 0.25 μm film) and FID.

## 3 Results

### 3.1 Characterization

Chemical composition of all laboratory prepared samples was determined by the ICP method. The results presented in Table 1 show chemical composition, i.e. molar ratio of zinc, magnesium and aluminium in the samples respectively. The specific surface area (BET) of dried and calcined Zn–Mg–Al samples decreased with the increasing Zn content in the sample in range of zinc content 0.80–2.11. As for zinc modified samples, the largest specific surface area is in the sample prepared by homogenous precipitation, which is caused by contribution of hydrozincite precipitated on the LDH surface. The low specific surface area of impregnated sample

**Table 1** Chemical and textural properties and methods of preparation of the samples

| Sample (dried/calcined) | Specific surface area SBET ($m^2$/g) | | Chemical composition (molar ratio) | | | Method of preparation |
|---|---|---|---|---|---|---|
| | 110 °C | 450 °C | Zn | Mg | Al | |
| ZMA-1/CZMA-1 | 83.0 | 205.7 | 0.26 | 2.93 | 1.00 | Coprecipitation |
| ZMA-2/CZMA-2 | 98.7 | 243.7 | 0.53 | 2.71 | 1.00 | Coprecipitation |
| ZMA-3/CZMA-3 | 96.0 | 238.4 | 0.80 | 2.45 | 1.00 | Coprecipitation |
| ZMA-4/CZMA-4 | 59.6 | 147.5 | 1.03 | 2.05 | 1.00 | Coprecipitation |
| ZMA-5/CZMA-5 | 45.6 | 122.3 | 1.55 | 1.54 | 1.00 | Coprecipitation |
| ZMA-6/CZMA-6 | 30.5 | 114.8 | 2.11 | 1.01 | 1.00 | Coprecipitation |
| ZMA-7/CZMA-7 | 73.5 | 214.2 | 0.48 | 3.10 | 1.00 | Kneading |
| ZMA-8/CZMA-8 | 10.0 | 175.3 | 0.52 | 3.14 | 1.00 | Impregnation |
| ZMA-9/CZMA-9 | 47.8 | 162.1 | 0.57 | 3.19 | 1.00 | Impregnation |
| ZMA-10/CZMA-10 | 96.2 | 192.6 | 0.55 | 2.61 | 1.00 | Homogenous precipitation |
| ZA/CZA | 18.1 | 105.1 | 3.02 | – | 1.00 | Coprecipitation |
| MA/CMA | 59.5 | 188.5 | – | 3.22 | 1.00 | Coprecipitation |
| Z/CZ | 51.6 | 16.7 | 1.00 | – | – | Precipitation |

ZMA-8 is connected with filling up the pores with the produced $Zn(OH)_2$. Having been calcined, the samples show an increase of the specific surface areas (up to the value of around 150–200 $m^2$/g). A less marked increase is observed in samples with high zinc content, whereas the sample Z, containing $Zn(OH)_2$, exhibits the opposite trend—after calcination, its specific surface area decreases significantly, which is connected with the formation of ZnO.

Diffractograms of dried samples (Fig. 1) exhibit typical diffraction lines characteristic for LDH materials. Typical are reflexions on 2theta 10.3°, 22.9°, 34.7°, 39.1°, 46.2°, 60.5° and 61.8°. Other crystallic phases present in the samples include zinc hydroxide contained in sample Z, typical diffraction lines 2theta 31.8°, 34.4°, 36.2° and 56.6°. A small part of zinc hydroxide is also formed in sample ZA, where the diffraction spectrum shows that not the entire zinc was built into the structure of LDH. Samples Z, ZMA-9 and ZMA-10 also contain, as a minority phase, hydrozincite with characteristic lines 2theta 13.0°, 28.0°,31.0°and 32.8°, while in sample ZMA-7 the added ZnO is visible.

Calcined samples (Fig. 2) indicate that magnesium oxide phase content (2θ 43.0°and 62.4°) decreases with the

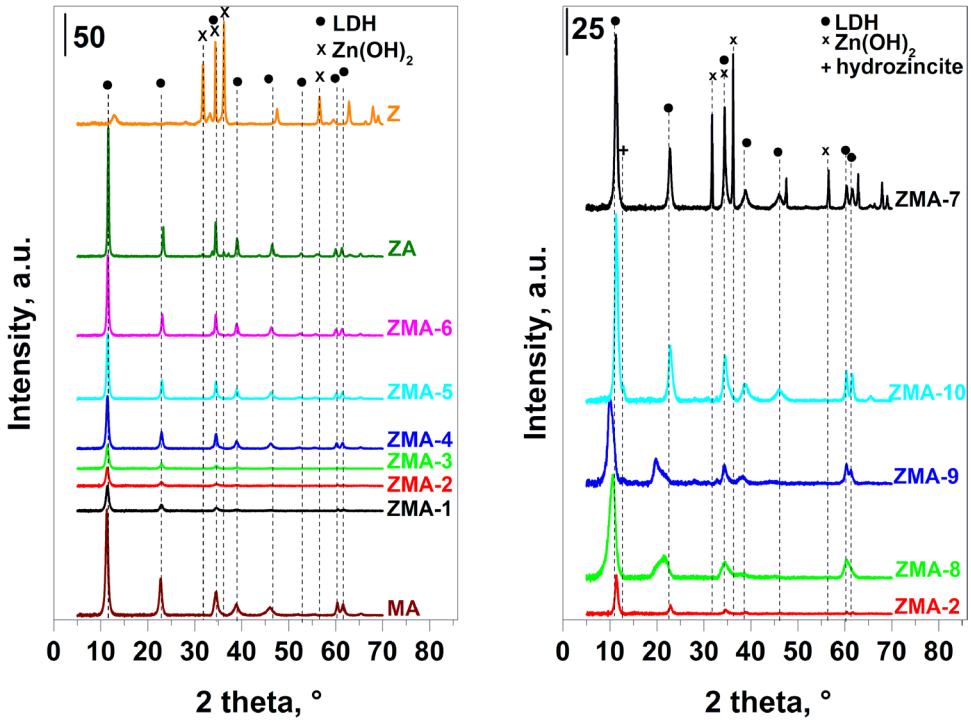


**Fig. 1** XRD patterns of the prepared dried Zn/Mg/Al samples

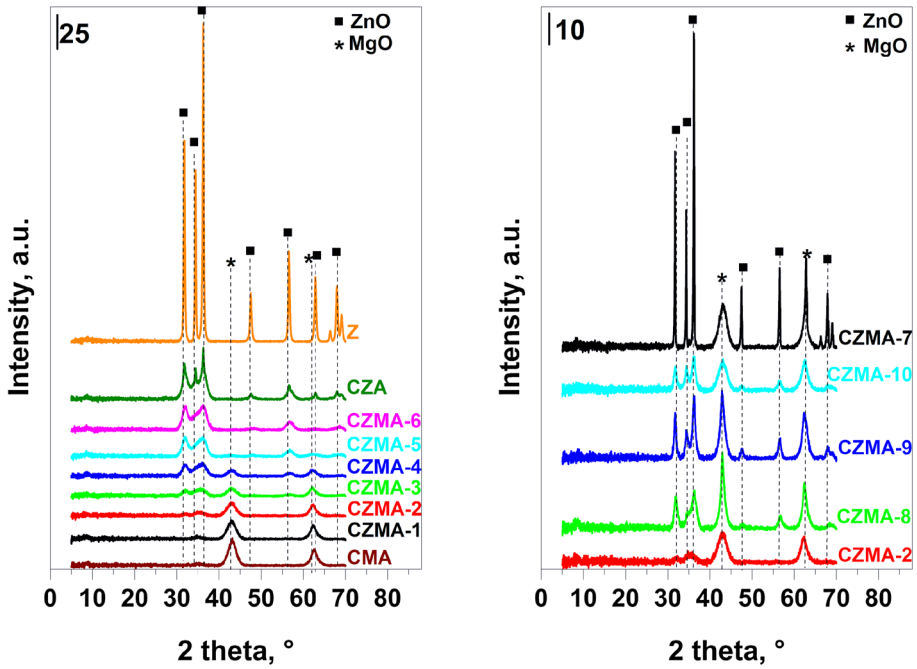


**Fig. 2** XRD patterns of the calcined Zn modified Mg/Al samples

increasing content of zinc in the sample. The highest crystallinity is exhibited by the sample Z containing only zinc oxide phase: 2θ 31.7°, 34.4°, 36.2°, 47.5°, 56.5°, 62.8° and 67.9°.

For samples containing LDH phase, the size of crystallites and interlayer distance of LDH phase were identified (Table 2). The size of crystallites of dried samples was calculated from the first distinctive LDH reflexion (around 11° 2θ). The interlayer distance of the samples does not change significantly, showing only a minor reduction with the increase of zinc content in the sample. The sample containing only Mg/Al LDH has an interlayer distance of 7.82 Å, while the Zn/Al LDH sample exhibits only slightly smaller value of 7.62 Å. As for zinc modified samples, a major increase was observed in the samples ZMA-8 and ZMA-9 prepared by impregnation with zinc nitrate, which is due to introduction of $NO_3^-$ anion into the interlayer of LDH [18]. The sample ZMA-9 prepared by impregnation of dried sample MA contains, besides LDH phase, also hydrozincite. Compared to the sample ZMA-10, the hydrozincite content is relatively higher, which is caused by higher content of amorphous phase in the sample, or higher crystallinity of the sample ZMA-10.

**Table 2** Diffraction and phase properties of the dried samples

| Sample | Relative content of crystallic phases (%) | | | | LDH crystallite size D (nm) | LDH D value (Å) |
|---|---|---|---|---|---|---|
| | LDH | $Zn(OH)_2$ | ZnO | $Zn_5(OH)_6(CO_3)_2$ | | |
| ZMA-1 | 100.0 | – | – | – | 138.0 | 7.75 |
| ZMA-2 | 100.0 | – | – | – | 138.0 | 7.76 |
| ZMA-3 | 100.0 | – | – | – | 142.3 | 7.75 |
| ZMA-4 | 100.0 | – | – | – | 174.0 | 7.75 |
| ZMA-5 | 100.0 | – | – | – | 196.9 | 7.72 |
| ZMA-6 | 100.0 | – | – | – | 236.2 | 7.69 |
| ZMA-7 | 84.1 | – | 19.1 | – | 159.3 | 7.81 |
| ZMA-8 | 100.0 | – | – | – | 55.3 | 8.33 |
| ZMA-9 | 86.9 | – | – | 13.1 | 61.8 | 8.89 |
| ZMA-10 | 95.7 | – | – | 4.3 | 124.3 | 7.78 |
| ZA | 95.7 | 4.3 | – | – | 284.2 | 7.62 |
| MA | 100.0 | – | – | – | 159.0 | 7.82 |
| Z | – | 100.0 | – | – | – | – |

The size of LDH crystallites (Table 2) in samples ZMA-1 through ZMA-6 grows with the increasing content of Zn. The zinc modified sample ZMA-7 exhibits the same size of crystallites as the original MA; this is caused by the fact that the ZnO added by kneading to the MA cake does not directly affect its structure and remains as a separate phase. Samples prepared by impregnation show a significant decrease in the size of crystallites, which relates to reconstruction and reorganisation of the structure during the impregnation process. In case of sample ZMA-10 prepared by homogeneous precipitation of zinc on the surface of MA sample, the crystallite is slightly smaller.

The size of crystallites of MgO and ZnO calcined samples (Table 3) were calculated from the reflexions at 32° 2θ for ZnO and 43° 2θ for MgO. The reflexion in the position of 32° 2θ was chosen for ZnO because in case of samples with lower zinc content the reflexions in the positions of 34°and 36° 2θ are overlapping/connected, making it impossible to determine the values with precision. For CZMA-1 through CZMA-4 the results show increase in the size of MgO crystallites with the increasing content of Zn in the sample. For samples CZMA-5 and CZMA-6 it is not possible to determine the size of MgO crystallites because the diffraction lines are not visible. Similar situation occurs with the determination of ZnO crystallites, where the samples CZMA-1 through CZMA-3 contain too little ZnO phase, and therefore the respective diffraction lines cannot be quantified. The size of ZnO crystallites in other samples in the line shows an increasing tendency with the increasing zinc content. For modified samples, the biggest ZnO crystallite is observed in sample CZMA-7, which was prepared by kneading of the MA sample with ZnO. Modified samples CZMA-8 through CZMA-10 have ZnO crystallites whose size is at the border between samples with zinc in structure and those with free ZnO, which is caused by occurrence of ZnO as a separate phase on the surface and in the pores of the prepared samples.

**Table 3** Diffraction and phase properties of the calcined samples

| Sample | Relative content of crystallic phases (%) | | Crystallite size D (Å) | |
|---|---|---|---|---|
| | MgO | ZnO | MgO | ZnO |
| CZMA-1 | 93.4 | 6.6 | 37.8 | – |
| CZMA-2 | 87.1 | 12.9 | 37.3 | – |
| CZMA-3 | 69.4 | 30.6 | 38.4 | – |
| CZMA-4 | 49.5 | 50.5 | 45.0 | 71.2 |
| CZMA-5 | 13.9 | 86.1 | – | 73.3 |
| CZMA-6 | 4.5 | 95.5 | – | 73.2 |
| CZMA-7 | 21.4 | 78.6 | – | 577.3 |
| CZMA-8 | 77.8 | 22.2 | – | 113.5 |
| CZMA-9 | 64.8 | 35.2 | – | 172.9 |
| CZMA-10 | 59.4 | 40.6 | – | 125.2 |
| CZA | – | 100.0 | – | 124.9 |
| CMA | 100.0 | – | 43.8 | – |
| CZ | – | 100.0 | – | 320.4 |

Zinc modified samples were also characterized by scanning electron microscope (series of scans in Fig. 3). Images with smaller magnification show agglomerates of individual LDH crystallites. Images of MA sample exhibit well developed leaf-like crystals with sharp edges, while samples modified by impregnation exhibit deformed wavy crystals—this applies namely to sample ZMA-8. Images of the sample prepared by homogeneous precipitation display tiny thin leaves of hydrozincite released on LDH surface.

The process of transformation of LDH structure into mixed oxides was investigated also by applying thermogravimetric analysis (Fig. 4). DTG curves of the analysed samples indicate several steps of decomposition, which are accompanied with loss of mass. Physically adsorbed water and the interlayer water are removed at 50–200 °C, surface $OH^-$ groups and decomposition of carbonates in the LDH interlayer are observed at 200–500 °C [12]. Samples containing Zn in LDH structure (ZMA-1 through ZMA-6) show increasing loss of mass with decreasing zinc content. DTG curves illustrate a visible shift of the first peak towards higher temperatures depending on the decreasing zinc content, as well as lower intensity of the second peak with the opposite trend, where the intensity decreases with the increasing content of zinc in the sample. This is due to higher number of OH– groups in the brucite layer of LDH, resulting in higher loss of mass at around 400 °C.

Zinc modified samples have similar characteristics as this series, only samples ZMA-8 and ZMA-9, prepared by impregnation, exhibit higher loss of mass at around 400 °C (Fig. 5). This relates to the decomposition of the nitrate anion present in the material after impregnation of the basic LDH with a solution of zinc nitrate. Mass detector has identified in ZMA-8 mainly the presence of nitrogen oxides originated from thermal decomposition of nitrate anion, while the sample ZMA-9 contained nitrogen oxides as well as $CO_2$, which resulted from thermal decomposition of carbonate anion (Fig. 10). As for ZMA-10 and the sample MA, which was used for the preparation of zinc modified samples, only $CO_2$ was detected. The content of $CO_2$ was higher in ZMA-10, which corresponds with the contribution of carbonate anion bound in hydrozincite. The presence of $NO_3^-$ anions was also proved by the DRIFT method.

The DRIFT analysis of LDH structure, or the mixed oxide, showed differences between the prepared samples and the modified samples (Figs. 6, 7). DRIFT spectra of the prepared materials are similar to other published results [18, 22–27].

The typical wide band at approximately 3400–3600 $cm^{-1}$ is attributed to the stretching vibrations of structural

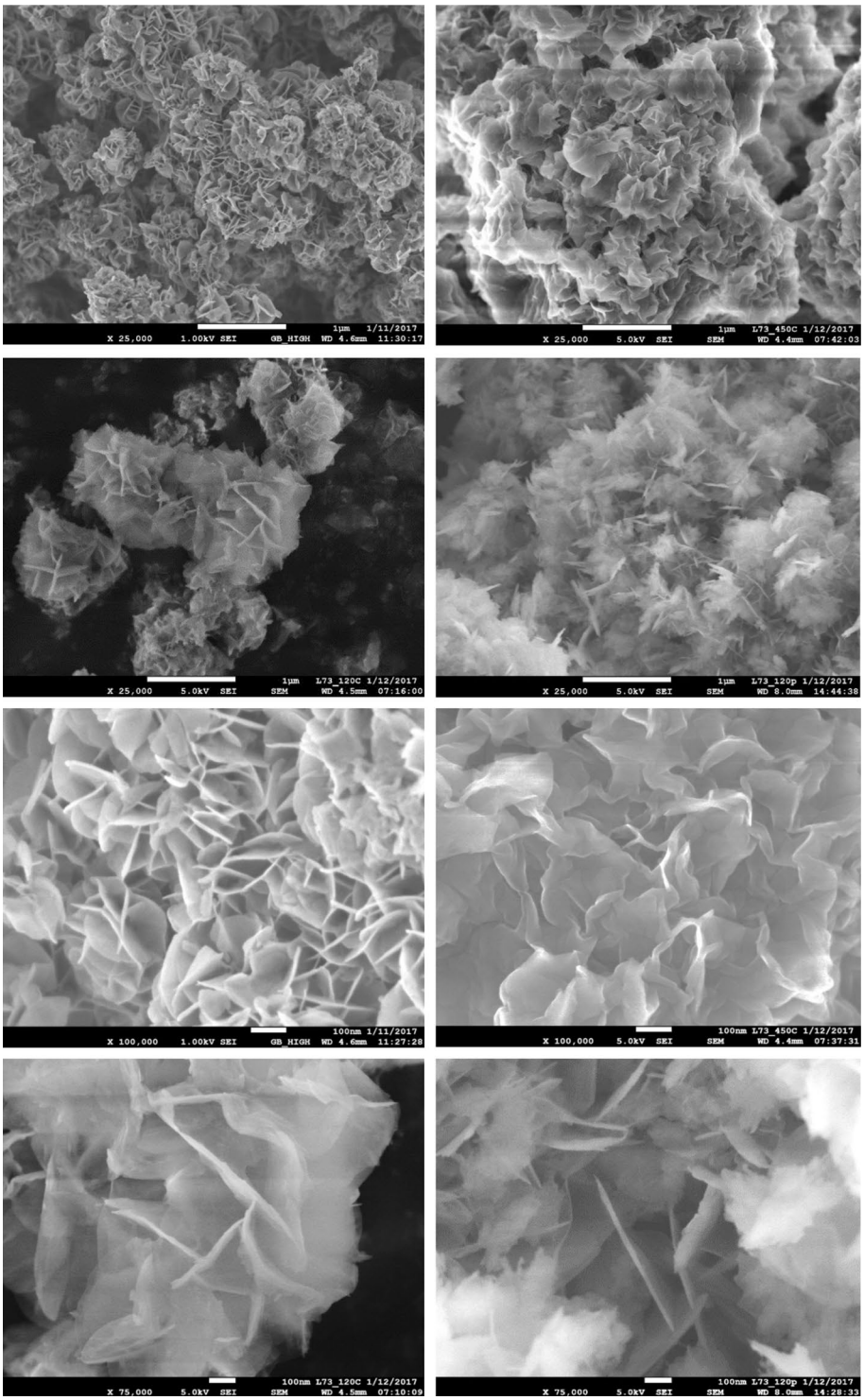


**Fig. 3** SEM images of the prepared samples—first quadruple (upper group) with lower resolution of 25,000× and second quadruple (lower group) with higher resolution of 75,000–100,000× (MA, ZMA-8, ZMA-9, ZMA-10)

hydroxyl groups in the brucite-like layer. The band around 1640 $cm^{-1}$ indicates the presence of water molecules in LDH and the bands 1380 and 1420 $cm^{-1}$ point to the presence of carbonates in the interlayer. The band around 1510 $cm^{-1}$ corresponds to the OH– absorption band, and the bands 820–840 and 1760 $cm^{-1}$ pertain to the nitrate anion. The area of low frequencies showed bands at 550, 680 and 770 $cm^{-1}$ related to M–OH vibrations, and the band at 420 $cm^{-1}$ assigned to O–M–O vibration. Calcination of the samples resulted in removal of water, carbonate and hydroxide anions; this was confirmed by disappearance or significant reduction of the respective bands at 1380, 1640 and the wide band 3400–3600 $cm^{-1}$. M–OH and O–M–O vibrations can be seen in the bands at 470, 680 and 790 $cm^{-1}$. DRIFT

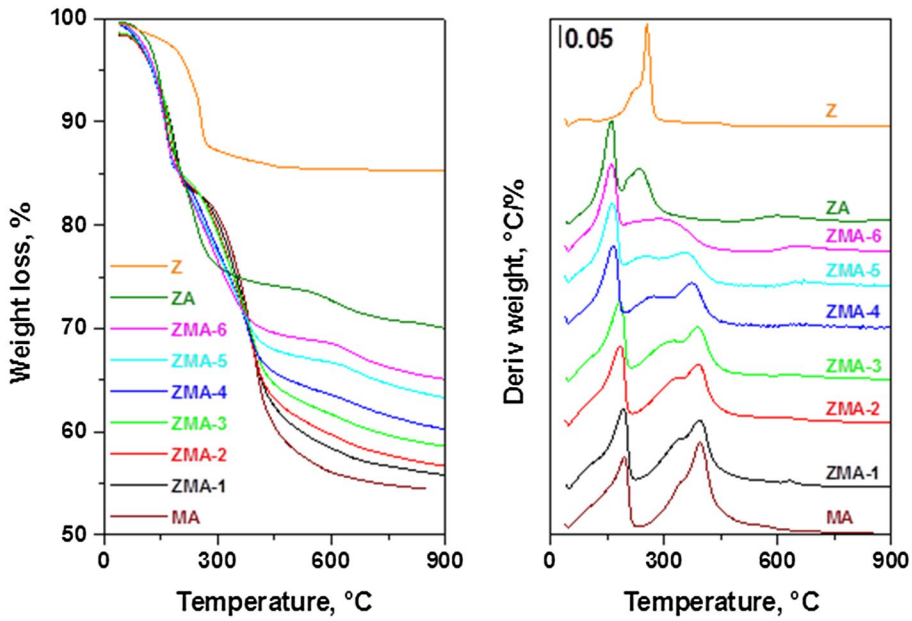


**Fig. 4** TGA (right)/ DTG (left) curves of the prepared samples

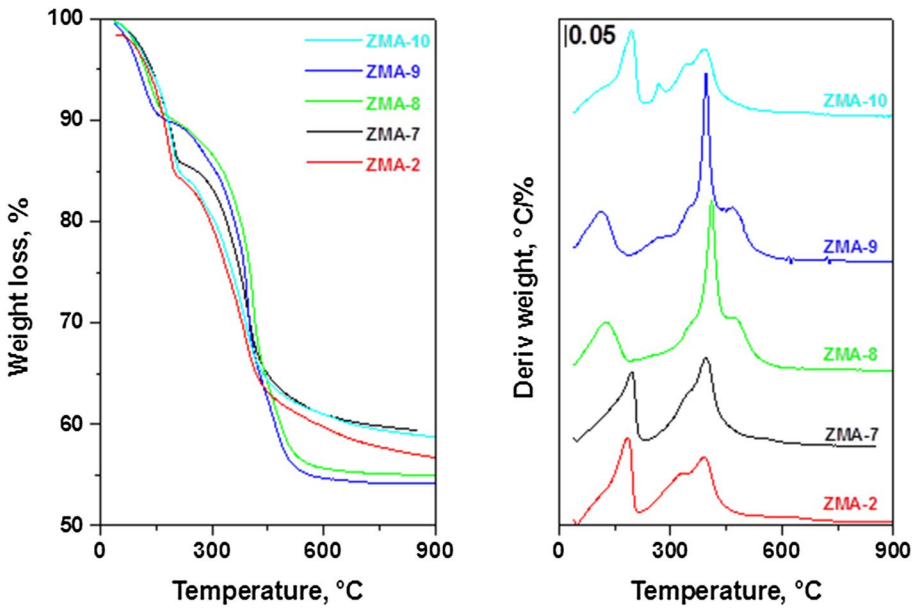


**Fig. 5** TGA (right)/ DTG (left) curves of the Zn modified Mg/Al samples

spectra of samples calcined at the temperature T = 450 °C indicate the presence of residual carbonate and hydroxyl anions. The presence of water sorbed from air during measurement of the samples is documented by a moderate band around 1640 $cm^{-1}$.

Acidic and basic properties were investigated by desorption of ammonia and carbon dioxide respectively (Figs. 8, 9). $NH_3$-TPD spectra show a broad peak, indicating the presence of weak and medium acid sites. CZ sample shows two separate peaks, one with the maximum at 95 °C caused by residual $NH_3$ bound to surface, while the other reaching the maximum at the temperature of 410 °C is probably caused by further thermal decomposition of the sample. Compared to CZMA-2, zinc modified samples have a narrower peak and the materials contain mainly weak acid sites. The density of acid sites in CMA, CZMA-1 through CZMA-6 and CZA samples increases with the content of Zn and is comparable to the density of acid sites in zinc modified samples.

$CO_2$-TPD spectra of the samples indicate the presence of at least three types of basic sites located in low temperature (100–110 °C), medium temperature (200–280 °C) and high temperature (300–350 °C) regions (the temperatures may be assigned to low, medium and strong basic sites). Samples CZMA-1 through CZMA-6 show higher rate of

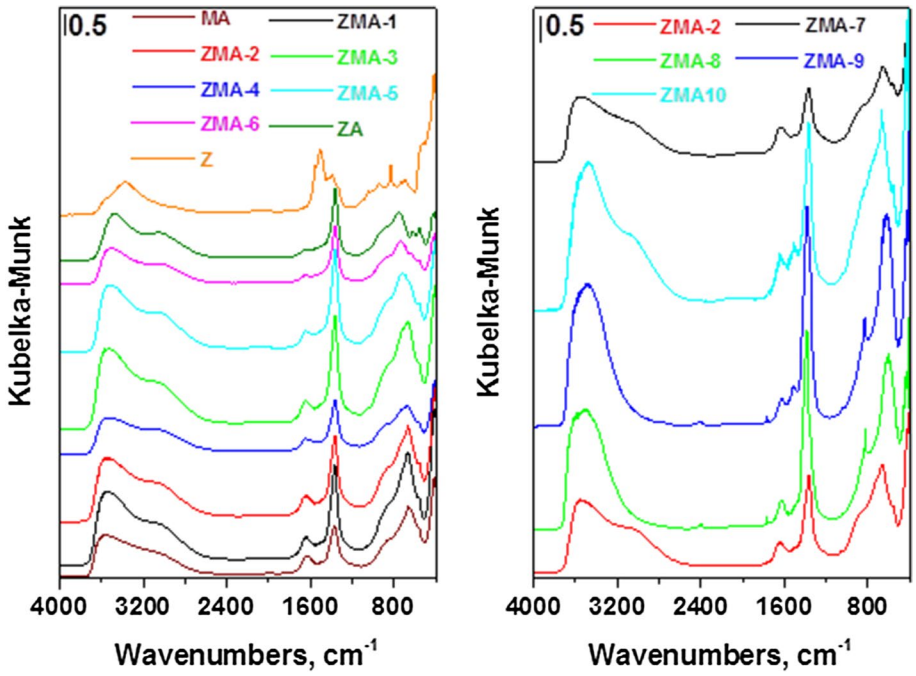


**Fig. 6** DRIFT spectra of the dried prepared samples (left) and of the dried Zn modified Mg/Al samples (right)

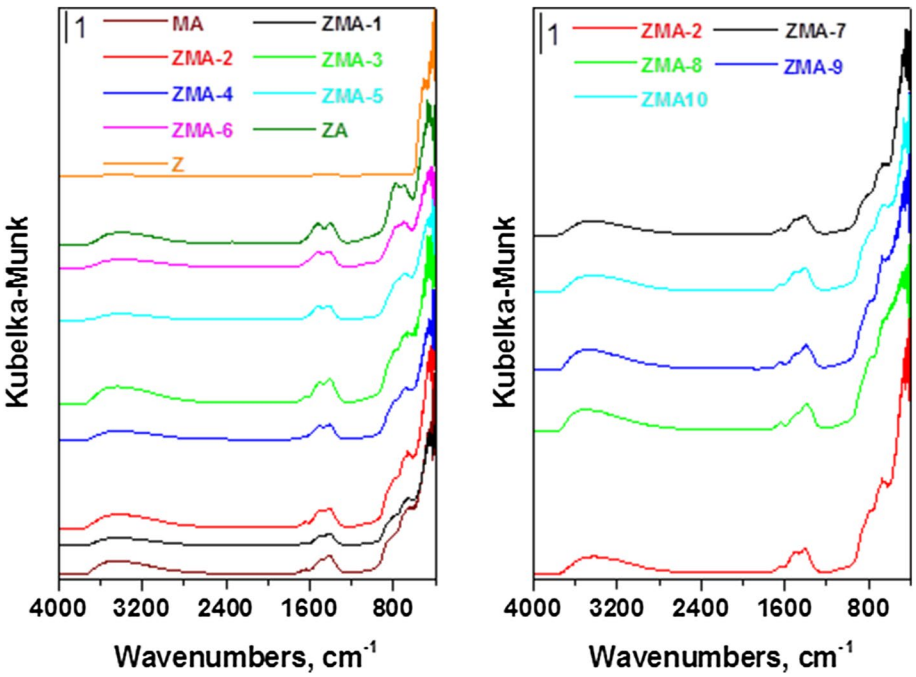


**Fig. 7** DRIFT spectra of the calcined prepared samples (left) and of the calcined Zn modified Mg/Al samples (right)

medium basic sites in comparison to sample CMA; with increasing zinc content the peak moves towards lower temperatures. As for sample CZA, there is no clear distinction between weak and medium basic sites, and sample CZ exhibits, similarly as $NH_3$-TPD, only two separate peaks—first at 105 °C caused by residual $CO_2$ bound on surface, and second at 420 °C which is probably caused again by further thermal decomposition of the sample.

Zinc modification of MA sample leads to a change in the ratio of the individual basic sites. Sample CZMA-7 contains more medium than weak basic sites, while in sample CZMA-9 the ratio is almost equal, and in sample CZMA-10 the ratio of weak and medium basic sites is opposite. In terms of density of basic sites, CZ is the most distinctive sample, which is due to very small specific surface area. The density of medium basic sites reaches the maximum in

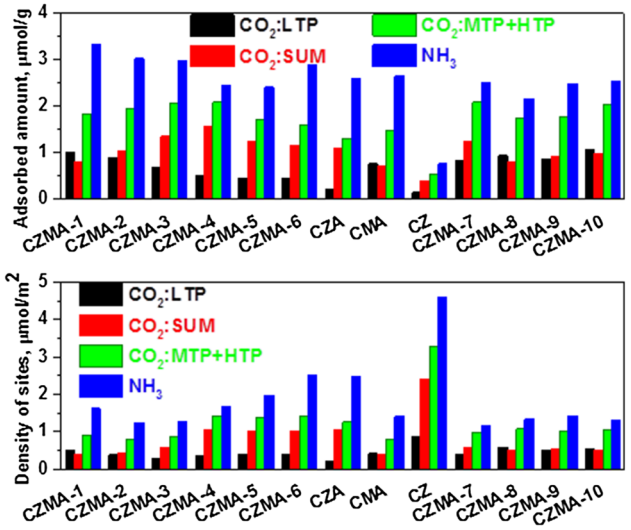


**Fig. 8** Concentration and density of acid and basic sites of the calcined samples. $NH_3$-TPD, $CO_2$-TPD [*LTP* low temperature peak (100–110 °C), *MTP* medium temperature peak (200–280 °C), *HTP* high temperature peak (300–350°C)]

sample CZMA-4. Zinc modified samples (CZMA-7 through CZMA-10) are very similar to each other. Compared to CZMA-2, they exhibit higher ratios, namely of weak basic centres.

Based on the obtained results it is obvious that the modified samples ZMA-8 and ZMA-9 are very similar to each other, although they were prepared from differently thermally treated MA samples (Fig. 10). During impregnation of dried LDH, $CO_3^{2-}$ anion is substituted by $NO_3^-$ anion, which then reacts, forming another minority crystalline phase—hydrozincite. An indistinctive band of OH groups (1505–1510 $cm^{-1}$) observed in DRIFT spectrum of sample ZMA-9 indicates OH groups related to the formation of hydrozincite. The only other sample where the same band is observed is ZMA-10, which contains hydrozincite as well [28]. During impregnation of calcined LDH, no other crystalline phase is observed, the interlayer contains for compensation of the charge only $NO_3^-$ anion, and zinc is dispersed in the sample, not forming further crystalline phases visible in XRD. The values of interplanar distance in samples ZMA-8 and ZMA-9 indicate that ZMA-8 contains in the interlayer only nitrate anion, whereas ZMA-9 has a nitrate anion and probably partially also a carbonate anion [18]. Both modified samples also have almost identical acidobasic properties, which is demonstrated in catalytic tests, where they achieve similar results and also the best conversions of heptanal and selectivity to the required product, i.e. jasmine aldehyde, of all tested samples.

Summary equation of impregnation of dried MA and hydrozincite formation

$$5Mg_6Al_2(OH)_{16}CO_3 \cdot 4H_2O + 5Zn(NO_3)_2 = 5Mg_6Al_2(OH)_{16}(NO_3)_2 \cdot 4H_2O + Zn_5(CO_3)_2(OH)_6 + 13H_2O + 3CO_2$$

Equations of impregnation of calcined MA

$$Mg_6Al_2O_9 + Zn(NO_3)_2 + 13H_2O = Mg_6Al_2(OH)_{16}(NO_3)_2 \cdot 4H_2O + Zn(OH)_2$$

### 3.2 Aldol Condensation

In this work, aldol condensation of benzaldehyde with heptanal (Fig. 11) was used to evaluate the activity of several types of zinc containing catalysts prepared by different techniques. In this type of reaction, two possible products can occur—a product of autocondensation of two heptanal molecules—2-pentylnon-2-enal (PN) or a product of mixed aldol condensation—2pentylcinnamylaldehyde (jasmine aldehyde, JA).

Catalysts with increasing zinc content were tested at 80 °C. At this temperature, a well-marked maximum was observed. The highest heptanal conversions were obtained using catalysts CZMA-2 and CZMA-3; the CZMA-2 catalyst was chosen to be tested also at higher temperatures (100 and 120 °C, Table 4). Subsequently, other samples with the same molar composition were prepared by different methods, and the catalytic activity of these samples was tested only at 100 °C (at this temperature the reference catalyst CZMA-2 had the conversion higher than 85%). The temperatures for catalytic testing were selected according to our previous work [16]. The stability of catalysts was studied. The leaching metals from catalysts were not determinate in products, therefore the catalysts were stable in aldol condensation of benzaldehyde with heptanal. The fact that this reaction is heterogeneously catalyzed was confirmed by hot filtration test. No reaction occurred when catalyst was filtered of reaction mixture.

Aldol condensation performed using catalysts prepared by copreciptation method (Fig. 12) showed that the catalyst with the lowest activity was pure zinc oxide. This catalyst possessed a remarkably lower reaction rate comparing other catalysts.

When comparing catalysts containing increasing amount of zinc to pure Mg–Al oxide (CMA catalyst), the reaction rate was almost the same in all cases except catalyst CZMA-6 with the highest zinc amount of all coprecipitated catalysts. When comparing selectivities to the products, in all cases (except pure zinc oxide, CZ cat.) more jasmine aldehyde than 2-pentylnon-2-enal originated. The highest JA/PN ratio was present in the case of pure Mg-Al mixed oxide, in case of catalysts containing zinc this JA/PN ratio was lower. This reaction (catalyzed using pure zinc oxide) resulted in significantly more autocondensation product than mixed aldol condensation product. These results show that

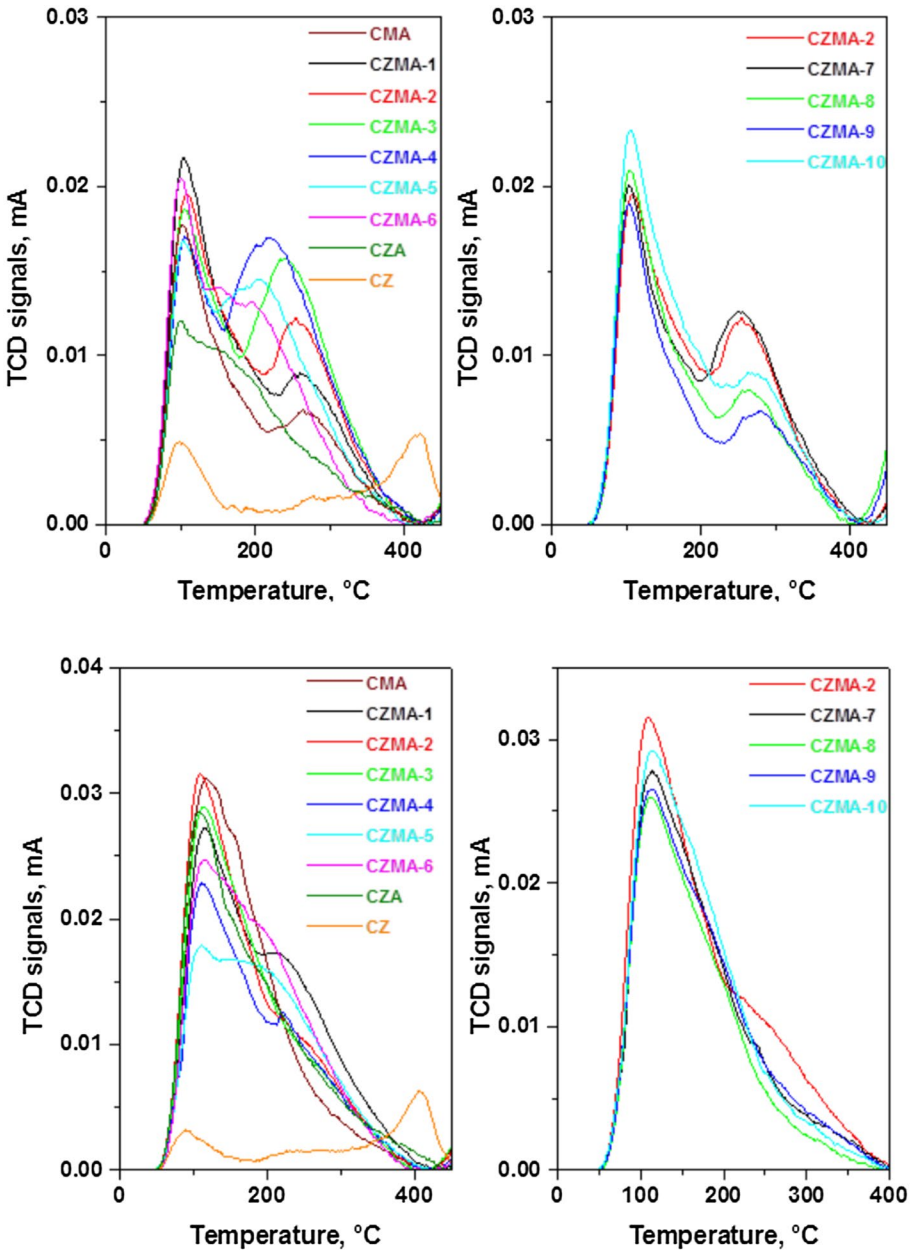


**Fig. 9** $CO_2$-TPD (up) and $NH_3$-TPD (down) graphs of the calcined samples

incorporation of zinc into the catalyst structure by coprecipitation did not influence the reaction rate and that the influence on selectivity to the desired mixed aldol product was rather negative.

### 3.2.1 Possible Reaction Mechanism

We propose the reaction mechanism based on literary data as follows: metal ($Mg^{2+}$) and oxygen in catalyst's structure interact with α-hydrogen of heptanal molecule (Fig. 13a) and generate initial hydroxyl group, which subsequently attacks other heptanal molecule and forms enolate. Enolate formed from heptanal attacks carbonyl group of benzaldehyde and forms aldol, which is subsequently dehydrated to aldol condensation product. Metal ($Al^{3+}$) and oxygen in catalyst's structure interacts with heptanal molecule (Fig. 13b) as well. In this case carbonyl group of heptanal is polarized by metal, which acidifies α-hydrogen and it is abstracted by framework oxygen generating metal enolate, which again attacks carbonyl group of benzaldehyde and reaction proceeds further as described below [29, 30].

### 3.2.2 Influence of Temperature

The influence of temperature on the reaction rate was predictable—with increasing temperature the reaction rate increased (Table 4).

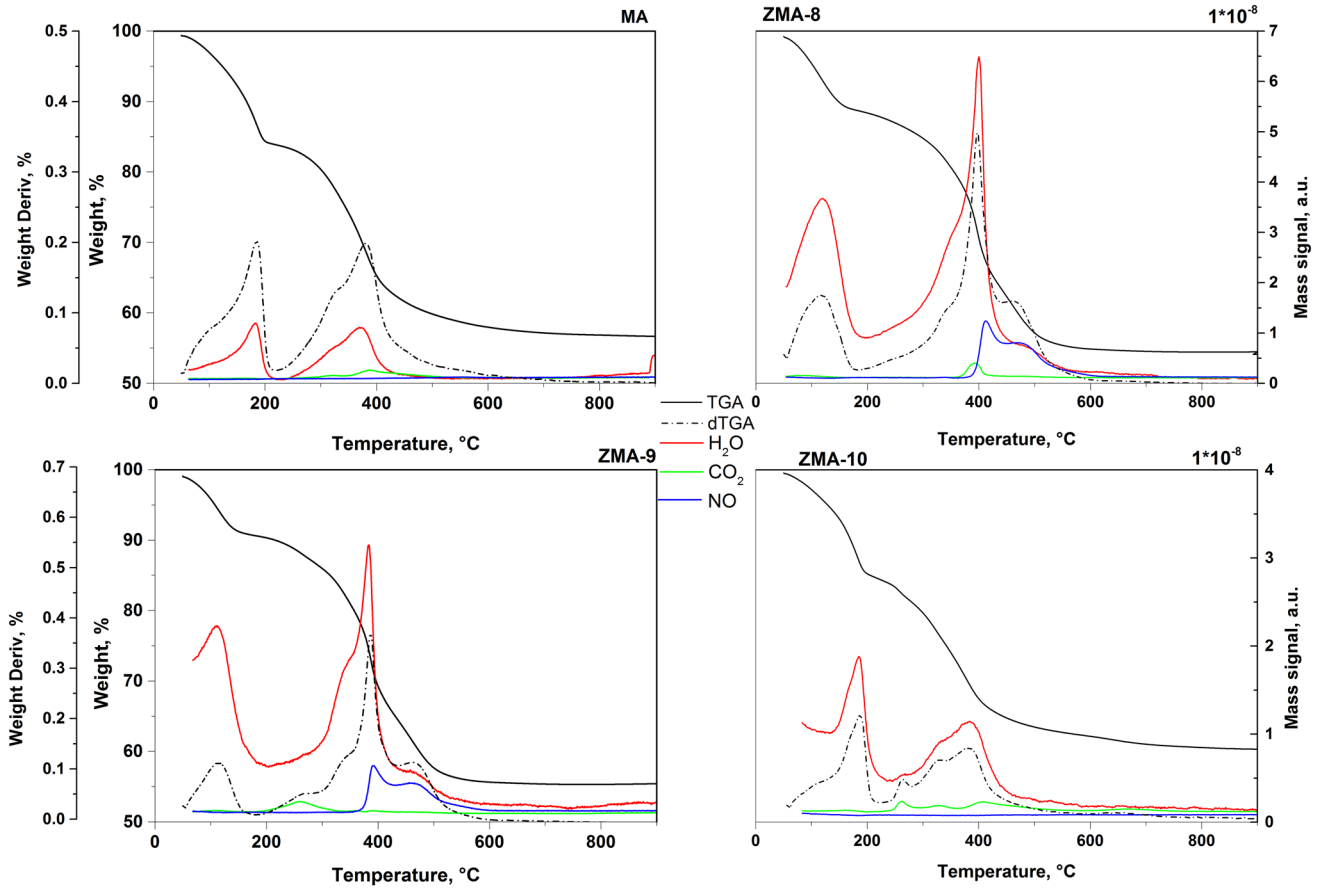


**Fig. 10** TGA-MS spectra of the MA sample and Zn modified Mg/Al samples (ZMA-8, ZMA-9 and ZMA-10)

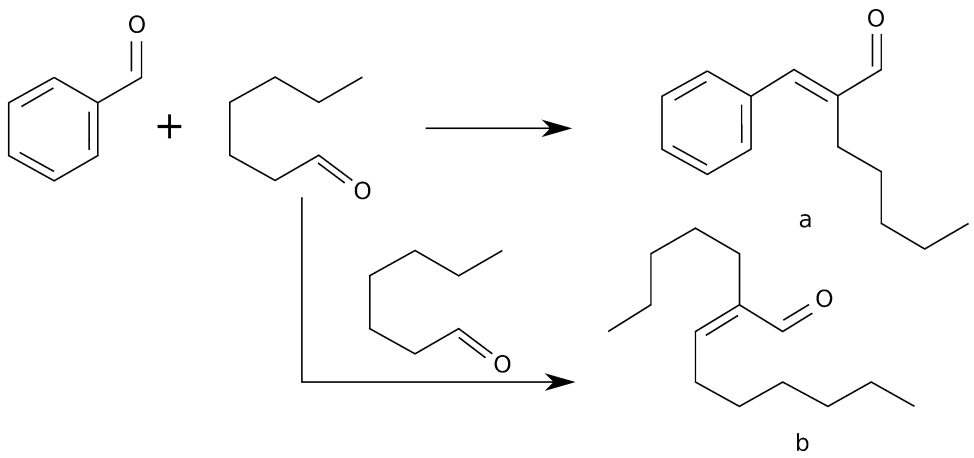


**Fig. 11** Reaction scheme of aldol condensation of benzaldehyde with heptanal giving 2-pentylcinnamylaldehyde (**a**) and 2-pentylnon-2-enal (**b**)

The reaction temperature also influenced the jasminaldehyde selectivity. In all cases the jasminaldehyde selectivity was increased from 57 to 71% with increasing temperature from 80 to 140 °C in heptanal conversion of 30%. The reaction rate was increased with increasing temperature. The heptanal conversion of 30% was achieved after 6.3 h at 80 °C and 0.89 h at 140 °C. This phenomenon could be also caused by the fact that with increasing temperature more heptanal refluxed, and therefore heptanal concentration in reaction mixture was lower, which caused preference of mixed product origination. The influence of temperature (60–160 °C) on conversion of heptanal and selectivity to jasmine aldehyde Prabhu at all studied [31] and Al-KIT-6 was used as acid catalysts. The rise of reaction temperature from 60 to 120 °C

**Table 4** Influence of temperature on the jasminaldehyde selectivity in 30% heptanal conversion (HP:BZ = 1:2 molar, catalyst CZMA-2, no solvent, 7 h)

| Temperature (°C) | Jasmine aldehyde selectivity (%) | Time (h) |
|---|---|---|
| 80 | 57 | 6.3 |
| 100 | 58 | 2.7 |
| 120 | 68 | 1.0 |
| 140 | 71 | 0.89 |

resulted in an increase in the conversion of heptanal and selectivity to jasmine aldehyde from 54 to 90% and from 70 to 90% respectively after 12 h. The reasons of the low concentration product of self-condensation of heptanal were the weak acid nature of Brönsted acid sites and the high content of benzaldehyde (molar ration benzaldehyde:heptanal 3:1) [31]. On the other hand, Hamza et al. [32] tested the FeAlP catalyst and found that with increased reaction temperature from 80 to 150 °C, the conversion of heptanal increased from 9 to 81%. The selectivity increased from 36 to 71% up to 140 °C. When the reaction was carried out at 150 °C, the selectivity decreased to 52% after 4 h. On contrary, Sharma et al. [9] presented that with increasing temperature from 70 to 170 °C the reaction rate increased as well. Mg–Al rehydrated mixed oxide with molar ratio Mg/Al 3.5 was used as catalyst. The selectivity to jasmine aldehyde decreased because higher temperature favors the formation of 2-pentylnon-2-enal, which is the product of self-condensation of heptanal [9]. However, we observed that the selectivity to jasmine aldehyde increased with increased reaction temperature, as shown in Table 4.

### 3.2.3 Influence of Zinc Amount in Catalyst and Type of Catalyst Preparation

Incorporation of zinc into the structure using coprecipitation method did not influence the selectivity to the desired product as it had been expected. For these modifications we used pre-prepared MA or CMA samples. All catalysts

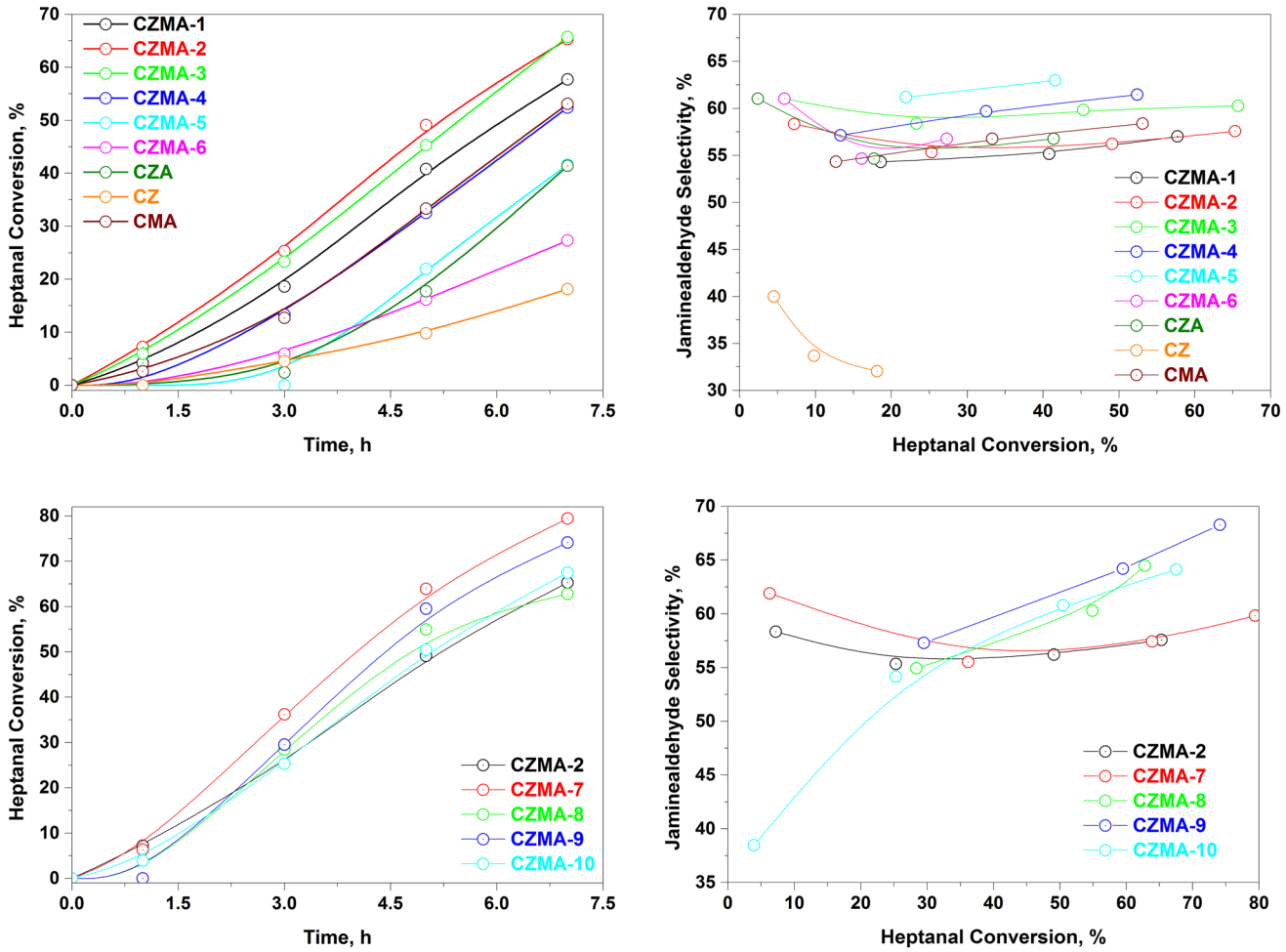


**Fig. 12** Conversion and selectivity (HP:BZ = 1:2 molar, 80 °C, no solvent, 7 h)

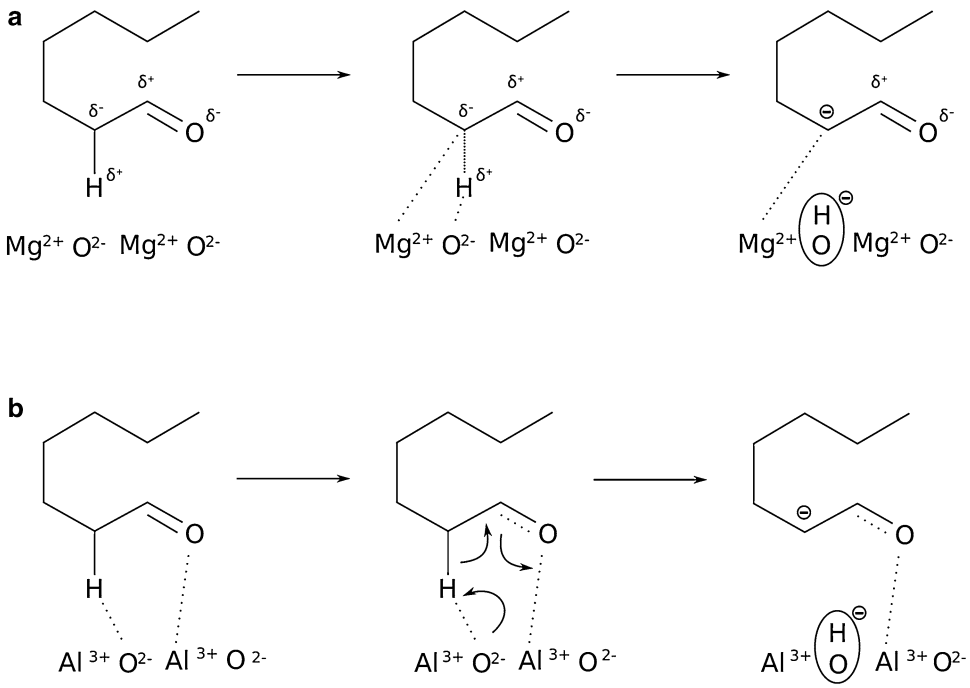


**Fig. 13** Enolate formation by Mg–Al catalyst from heptanal molecule

**Table 5** Jasmine aldehyde selectivity and time to reach 15% heptanal conversion (HP:BZ = 1:2 molar, 80 °C, no solvent)

| Sample | Jasmine aldehyde selectivity (%) | Time (h) |
|---|---|---|
| CZMA-1 | 54 | 2.4 |
| CZMA-2 | 57 | 1.8 |
| CZMA-3 | 60 | 2.0 |
| CZMA-4 | 57 | 3.7 |
| CZMA-5 | 60 | 4.3 |
| CZMA-6 | 56 | 4.7 |
| CZA | 56 | 4.6 |
| CZ | 33 | 6.2 |
| CMA | 55 | 3.7 |

**Table 6** Jasmine aldehyde selectivity and time to reach 40% heptanal conversion (HP:BZ = 1:2 molar, 80 °C, no solvent)

| Sample | Jasmine aldehyde selectivity (%) | Time (h) |
|---|---|---|
| CZMA-2 | 56 | 4.0 |
| CZMA-7 | 57 | 3.1 |
| CZMA-8 | 57 | 3.7 |
| CZMA-9 | 60 | 3.5 |
| CZMA-10 | 58 | 4.0 |

contained similar Mg:Al:Zn molar ratio (3:1:0.5). The highest initial reaction rates were observed at CZMA-2 and CZMA-3, how it can see on Fig. 12. CZMA-2 and CZMA-3 achieved also the highest heptanal conversion (65.3%) after 7 h.When comparing catalyst prepared by coprecipitation (CZMA-2) with catalysts prepared by other methods, coprecipitated catalyst showed significantly lower selectivity to cross-aldol product. Overall, the selectivity to cross-aldol product was the highest using materials prepared by impregnation. Catalyst activity was evaluated using isoconversion data (Tables 5, 6). Catalysts prepared by coprecipitation method were compared at 15% heptanal conversion. The highest selectivity to jasmine aldehyde was obtained using CZMA-5 catalyst, which was in the range of measurement error with the selectivities obtained using CZMA-2, CZMA-3 and CZMA-4 catalysts. Selectivity to jasmine aldehyde was similar also using other coprecipitated catalysts except CZ, which possessed significantly lower selectivity to jasmine aldehyde (33%). The highest reaction rate was obtained using CZMA-3 and CZMA-2 catalysts. Except for catalyst CZMA-1, coprecipitated catalysts showed a decrease of reaction rate with increasing zinc content.

Catalysts prepared by other ways of zinc incorporation were evaluated at 40% heptanal conversion. In this case, selectivity to jasmine aldehyde was in the range of measurement error for catalysts prepared by other synthesis methods than coprecipitation. Except catalyst CZMA-7, fairly lower catalyst activity was observed as well.

Correlation of catalysts (Fig. 14) indicates that the increasing zinc amount in catalyst caused the increase of jasmine aldehyde yield up to molar ratio Zn:Mg:Al = 0.5:2.5:1 (CZMA-2). With following increase of zinc amount in the catalyst, jasmine aldehyde yield decreased from 26 to 3%

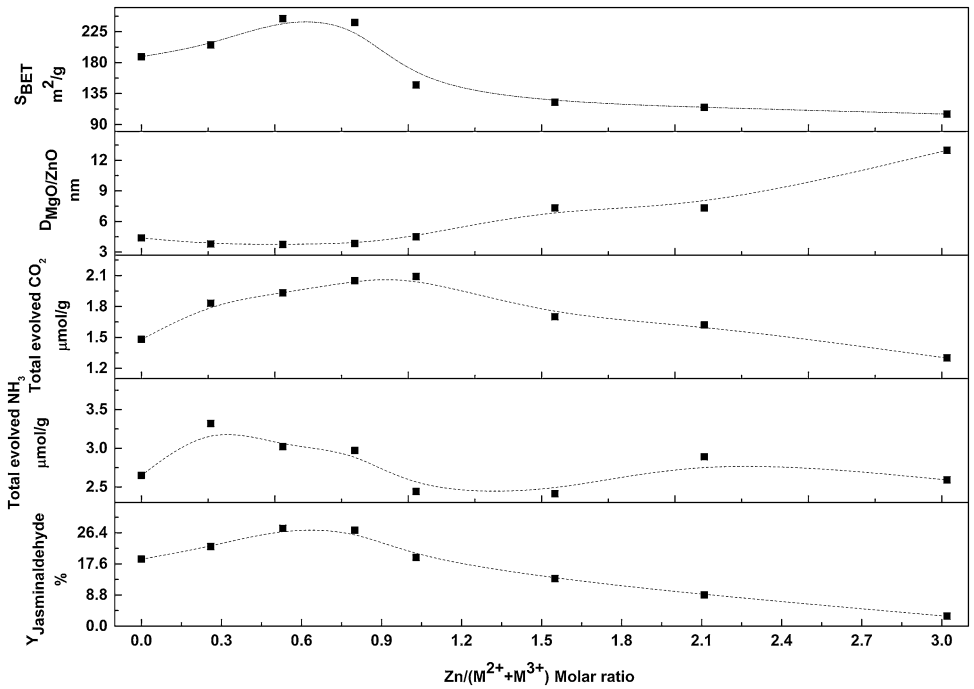


**Fig. 14** Correlation of catalyst characteristics and yield (HP:BZ = 1:2 molar, 80 °C, no solvent, 7 h)

for pure Zn-Al (molar ratio Zn:Al = 3:1, CZ) catalyst. The same trend was observed also in case of specific surface area ($S_{BET}$). Data of material basicity and acidity confirmed that both basic and acid sites are active in aldol condensation as predicted. More acid active sites were detected in materials with lower zinc amount, in case of basic active sites the maximum was observed in materials with molar Zn:Mg:Al ratio 1:2:1. A decrease of abundance of both acid and basic active sites was observed with higher zinc content in catalyst. This decrease was probably caused by the increase of particle size with increasing zinc amount, which caused decrease of specific surface area and was accompanied by decrease of amount of active sites.

Comparison with similar catalysts in literature was performed (Table 7). The results presented here are comparable with the data presented in literature for Mg-Al mixed oxides and better than chitosan modified hydrotacites or magnesium organo silicates.

## 4 Conclusion

Several catalyst types were synthesized and characterized using different methods. These materials with different Mg:Al:Zn ratio (1.0:2.1:1.0–3.2:0.57:1.0) were used as catalysts in aldol condensation of benzaldehyde with heptanal as a model reaction. Comparing the activity of pure Mg–Al oxide and Mg–Al–Zn oxides shows under the same conditions, yields of jasmine aldehyde by 15–20% higher. The amount of zinc in the catalyst influences the reaction rate, and the yields of jasmine aldehyde at 100 °C is in the range of 0.6–0.65. Increase of reaction temperature caused the increased reaction rate and also the origination of jasmine aldehyde in higher ratio. Contrariwise, usage of solvent (DMF) caused lower reaction rate and also decrease of jasmine aldehyde origination, but it is convenient to reduce the viscosity of the mixture in the event of synthesis in a flow reactor. It was shown that by modification by Zn it

**Table 7** Comparison with data in literature

| Catalyst type | Heptanal conversion (%) | Selectivity to jasmine aldehyde (%) | HP:BZ molar ratio | Temperature (°C) | Time (h) | References |
|---|---|---|---|---|---|---|
| Reconstructed Mg–Al hydrotalcite | 53 | 84 | 1:5 | 100 | 2 | 9 |
| Mg–Al mixed oxide | 99 | 75 | 1:5 | 125 | 8 | 8 |
| Magnesium organo silicate | 98 | 66 | 1:2 | 125 | 8 | 4 |
| Mg–Al mixed oxide | 99 | 73 | 1:2 | 100 | 7 | 16 |
| Chitosan grafted hydrotalcite | 97 | 61 | 1:2 | 125 | 7 | 33 |
| Mg–Al mixed oxide modified with zinc | 98 | 74 | 1:2 | 100 | 7 | Current work |

is possible to prepare catalysts, which are more active and provide higher yields of the desired product—jasmine aldehyde. Catalyst testing gave valuable data, which will help in further investigation of this reaction and in future testing in continuous stirred-tank reactor.

**Acknowledgements** The publication is a result of the project Reg. No. TH01011223, which was financially supported by TACR. The project has been integrated into the National Programme for Sustainability I of the Ministry of Education, Youth and Sports of the Czech Republic through the project Development of the UniCRE Centre, project code LO1606.

**Funding** Financial support from specific university research (MSMT No 20-SVV/2017).

## Compliance with Ethical Standards

**Conflict of interest** The authors declare that they have no conflict of interest.

## References

1. Abbaspourrad A, Kalbasi RJ, Zamani F (2010) Chin J Chem 28:2074
2. Ganga VSR, Abdi SHR, Kureshy RI, Khan NU, Bajaj HC (2016) J Mol Catal A 420:264
3. Tayade KN, Mishra M (2013) Catal Sci Technol 3:1288
4. Sharma SK, Patel HA, Jasra RV (2008) J Mol Catal A 280:61
5. Adwani JH, Khan NH, Shukla RS (2015) RSC Adv 5:94562
6. Vrbkova E, Vyskocilova E, Krupka J, Cerveny L (2016) Prog React Kinet Mech 41:289
7. Hajek J, Vandichel M, Van de Voorde B, Bueken B, De Vos D, Waroquier M, Van Speybroecka V (2016) J Catal 331:1
8. Sharma SK, Parikh PA, Jasra RV (2008) J Mol Catal A 286(1–2):55
9. Sharma SK, Parikh PA, Jasra RV (2010) Appl Catal A 386(1–2):34
10. Chunxiang M, Gang L, Zhenlu W, Yufei L, Jing Z, Wenxiang Z, Mingjun J (2009) React Kinet Mech Catal 98:149
11. Abelló S, Medina F, Tichit D, Pérez-Ramírez J, Groen J, Sueiras J, Salagre P, Cesteros Y (2005) Chemistry 11:728
12. Hora L, Kikhtyanin O, Čapek L, Bortnovskiy O, Kubička D (2015) Catal Today 241:221
13. Paterová I, Vyskočilová R, Červený L (2012) Top Catal 55:873
14. Xu J, Cao Y, Ma Q, Peng X (2013) Asian J Chem 25:3847
15. Shiauo S, Ko A (2006) J Chin Chem Soc 54:1539
16. Vrbková E, Tišler Z, Vyskočilová E, Kadlec D, Červený (2018) J Chem Technol Biotechnol 93(1):166
17. Hernandez WY, Alic F, Verberckmoes A, Van der Voort P (2017) J Mater Sci 52:628
18. Cavani F, Trifiro F, Vaccari A (1991) Catal Today, 11:173
19. Casenave S, Martinez H, Guimon C, Auroux A, Hulea V, Cordoneanu A, Dumitriu E (2001) Thermochem Acta 379:85
20. Jakubíková V, Kovanda F (2010) Chem Listy 104:900
21. Kustrowski P, Sułkowska D, Chmielarz L, Dziembaj R (2006) Appl Catal A 302:317
22. Diko M, Ekosse G, Ogola J (2016) Acta Geodyn Geomater 13(2):149
23. Kikhtyanin O, Tišler Z, Velvarská R, Kubička D (2017) Appl Catal A 536:85
24. Wahab R, Ansari SG, Kim YS, Dar MA, Shin H (2008) J Alloys Compd 461:66
25. Lu HF, Qi T, Yan SL, Liang B (2010) Biotechnol Adv 28(5):620
26. Kloprogge JT, Hickey L, Frost RL (2004) J Raman Spectrosc 35(11):967
27. Saikia BJ, Parthasarathy G (2010) J Mod Phys 1:206
28. Lin Z, Guo F, Wang C, Wang X, Wang K, Qu Y (2014)) RSC Adv 4(4):5133
29. Lewis JD, Vyver S, Roman-Leshkov Y (2015) Angew Chem Int Ed 54:9835
30. Tanabe K, Misono M, Httori H, Ono Y (1990) New solid acids and bases their catalytic properties. Elservier, New York
31. Prabhu A, Palanichamy M (2013) Microporous Mesoporous Mater 168:126
32. Hamza A, Nagaraju N (2015) Chin J Catal 36:209